PNAS RESEARCH ARTICLE | APPLIED BIOLOGICAL SCIENCES OPEN ACCESS

# Circular RNA lipid nanoparticle vaccine against SARS-CoV-2

Kelsey L. Swingle[a,1], Alex G. Hamilton[a,1], Xuexiang Han[a], Kuo-Chieh Liao[b], Hannah C. Safford[a], Ajay S. Thatte[a], Hannah C. Geisler[a], Junchao Xu[a], Tzuen Yih Saw[b], Yue Wan[b], and Michael J. Mitchell[a,c,d,e,f,g,h,i,2]

Affiliations are included on p. 11.

Edited by Chad Mirkin, Northwestern University, Evanston, IL; received March 12, 2025; accepted July 15, 2025

**With the advent and widespread use of messenger RNA (mRNA) vaccines against severe acute respiratory syndrome coronavirus 2 (SARS-CoV-2), RNA vaccines have emerged as an exciting class of vaccine offering low cost, rapid development, and high modularity and manufacturability. Protein-coding circular RNA (circRNA) is an emerging class of RNA cargo that offers increased stability compared to mRNA with potentially reduced immunogenicity, but delivery technologies for intracellular delivery of circRNA remain underexplored. Here, we develop an optimized lipid nanoparticle (LNP) platform for circRNA delivery to immune cells, observing strong and durable transgene expression in vitro and in vivo. We employ a design-of-experiments (DoE) methodology to identify key formulation parameters for enhanced circRNA delivery and, upon intramuscular administration of our optimized circRNA LNPs to mice, observe substantial accumulation within draining lymph nodes and strong dendritic cell (DC) maturation at short time points. Applying this optimized circRNA LNP platform to vaccination against SARS-CoV-2, we demonstrate robust antibody production and enhanced immune responses in mice compared to vaccination with mRNA LNPs, including strong $T_h1$-biased cellular responses and a 3.8-fold increase in antigen-specific reciprocal endpoint IgG titers. These results provide insights into design criteria for circRNA LNP formulations and support the use of circRNA LNPs for vaccination against infectious diseases.**

RNA | vaccine | lipid nanoparticle | SARS-CoV-2 | circular RNA

## Significance

Protein-coding circular RNA (circRNA) is an exciting RNA cargo capable of inducing strong protein production with greater durability of expression than linear species such as messenger RNA (mRNA). There is a dearth of literature describing the refinement of existing RNA delivery technologies for the effective encapsulation and delivery of this emerging cargo. Lipid nanoparticles (LNPs) are the preeminent nonviral RNA delivery technology, as demonstrated by the Pfizer/BioNTech and Moderna mRNA LNP vaccines against SARS-CoV-2. However, these vaccines were enabled by years of refining LNPs for use with bulkier mRNA cargo. This study identifies key LNP formulation parameters for circRNA encapsulation and delivery and applies these insights to the development of a circRNA LNP vaccine against SARS-CoV-2.

Messenger RNA (mRNA) lipid nanoparticle (LNP) vaccines against severe acute respiratory syndrome coronavirus 2 (SARS-CoV-2) have seen widespread deployment during the COVID-19 pandemic, proving themselves both safe and highly effective at reducing disease-associated morbidity and mortality (1, 2). These RNA vaccines offer low production costs with unprecedentedly rapid development and manufacturing (3). Furthermore, vaccination platforms based on RNA possess a high degree of modularity, which has spurred numerous investigations into the development of RNA vaccines against influenza and other infectious diseases (4, 5).

Circular RNA (circRNA) is an emerging RNA cargo, unique in that it is covalently closed. circRNA is substantially more stable than linear RNA species in the cell due to its resistance to exonuclease-mediated degradation, allowing more durable transgene expression than mRNA (6, 7). This potential for durable gene expression is attractive both for protein replacement therapies and for vaccination, providing a potential route for dose sparing (8, 9). Furthermore, while nucleoside modification of exogenous mRNA is essential to reduce its immunogenicity to manageable levels (10, 11), protein-coding circRNA has no such requirement, demonstrating low immunogenicity even with only canonical nucleosides (7), a favorable attribute for manufacturability. Just as the advent of nucleoside modification enabled the present mRNA renaissance, so too have recent advances in RNA synthesis and circularization enabled advances in circRNA technology, leading to renewed interest in circRNA as a new class of RNA for therapeutics and vaccines (6, 12).

As circRNA is a relatively new class of RNA payload, drug delivery technologies tailored for the cargo have yet to emerge. Like other RNA types, circRNA is a fragile payload, sensitive to abundant endogenous nucleases and unable to transit the cell membrane by itself due to its negative charge (9). While previous studies have effectively encapsulated and delivered circRNA using LNPs, most investigators have simply adopted LNP formulation parameters previously optimized for mRNA or small interfering RNA (siRNA) delivery (7, 13–15), and the development of design criteria for circRNA LNP formulations remains an underexplored area. As reoptimization of historical siRNA LNP formulations for mRNA delivery previously resulted in substantial improvements in mRNA transfection (16), there is reason to think that the development of circRNA-tailored LNP formulation parameters could provide enhanced circRNA transfection.

Author contributions: K.L.S., A.G.H., and M.J.M. designed research; K.L.S., A.G.H., X.H., H.C.S., A.S.T., H.C.G., and J.X. performed research; X.H., K.-C.L., T.Y.S., and Y.W. contributed new reagents/analytic tools; K.L.S. and A.G.H. analyzed data; and K.L.S., A.G.H., and M.J.M. wrote the paper.

Competing interest statement: X.H. and M.J.M. are inventors on a U.S. provisional patent application related to some of the ionizable lipids used in this article.

This article is a PNAS Direct Submission.



[1]K.L.S. and A.G.H. contributed equally to this work.

[2]To whom correspondence may be addressed. Email: mjmitch@seas.upenn.edu.

This article contains supporting information online at https://www.pnas.org/lookup/suppl/doi:10.1073/pnas.2505718122/-/DCSupplemental.

Published September 15, 2025.

In this work, we identify an ionizable lipid capable of strong immune cell circRNA transfection in vitro and in vivo, outperforming clinical standard ionizable lipids. We perform iterative design-of-experiments (DoE) optimization of LNP formulation parameters with this ionizable lipid to further improve LNP-mediated circRNA transfection by up to 20-fold, identifying key design parameters for effective circRNA encapsulation and delivery. We administer our optimized circRNA LNPs to mice and note LNP accumulation in antigen-presenting cells (APCs) in draining lymph nodes and strong transfection within secondary lymphoid tissues. Finally, we evaluate our optimized circRNA LNP formulation for immunization against SARS-CoV-2 variant B.1.617.2 (Delta) in mice, demonstrating enhanced immune responses compared to mRNA LNPs, including a 3.8-fold increase in antigen-specific reciprocal endpoint serum IgG titers.

## Results

**LNPs Formulated with Ionizable Lipid 12D6.2 Effectively Deliver Circular RNA Cargo.** While circRNA delivery using LNPs has been reported previously, relatively little optimization of the lipid components has been performed, with the bulk of previous optimization work focusing on the RNA cargo (6, 7, 17). As different nucleic acid cargoes have demonstrated varying optima in lipid makeup for cargo delivery (16, 18), we reasoned that tailoring LNPs for circRNA could yield improved encapsulation and transfection characteristics compared to simply adopting existing LNP formulations optimized for mRNA delivery. As a starting point for circRNA LNP optimization, we first sought to identify an ionizable lipid capable of facilitating circRNA transfection in immune cells. Our group has previously reported immune cell transfection with mRNA using the piperazine-derived ionizable lipids C14-482, C14-488, and C14-494 (19–22), so we evaluated these lipids for circRNA delivery. We also evaluated the biodegradable ionizable lipids 5D6.2 (23), 8D6.2 (23), 12D6.2 (23), 12T-O14 (24), and 11-10-8 (25), previously explored for hepatic gene editing applications. We compared all nine ionizable lipids against three clinical LNP formulations: Spikevax (Moderna), an mRNA LNP formulation containing the SM-102 ionizable lipid; Comirnaty (Pfizer/BioNTech), an mRNA LNP formulation containing the ALC-0315 ionizable lipid; and Onpattro (Alnylam), an siRNA LNP formulation containing the DLin-MC3-DMA (MC3) ionizable lipid.

We formulated LNPs encapsulating circRNA encoding the NanoLuc engineered luciferase using microfluidic mixing. After assessing size distribution and entrapment efficiency of the resultant LNPs (*SI Appendix*, Table S1), we transfected DC2.4 murine dendritic cells (DCs), Jurkat human T cells, and RAW 264.7 murine macrophages and assessed bioluminescence 24 h later using a plate reader. In all immune cell lines tested, novel ionizable lipids substantially outperformed clinical controls in terms of circRNA transfection (Fig. 1 *A*–*C*). Of particular note were the ionizable lipids C14-488, C14-494, 5D6.2, and 12D6.2, each of which significantly outperformed MC3 for circRNA transfection in at least two of the three cell lines tested.

As relationships between in vitro and in vivo LNP performance are often weak (26), we further evaluated the performance of our candidate circRNA LNPs in vivo. Twelve hours after *i.m.* administration of NanoLuc circRNA LNPs to mice, we performed whole-body bioluminescence imaging to evaluate transfection profiles (Fig. 1 *D* and *E*). Here, we identified C14-482, 5D6.2, 8D6.2, 12D6.2, SM-102, and ALC-0315 as promising candidate ionizable lipids for in vivo circRNA transfection. Notably, the C14-488 ionizable lipid, which emerged as a lead candidate from in vitro screening, demonstrated poor in vivo performance, establishing its status as a false positive and underscoring the importance of in vivo validation of LNP performance. Conversely, the ALC-0315 and SM-102 lipids, which performed poorly in vitro, demonstrated moderate-to-strong in vivo transfection, making them apparent examples of false negatives and poor candidates for subsequent in vitro LNP optimization experiments. However, several ionizable lipids emerged as true positives, demonstrating strong transfection both in vitro and in vivo (Fig. 1*F*). While some of these (C14-482, 8D6.2) demonstrated clear transfection of the liver, 12D6.2 LNPs demonstrated apparent transfection of the lymph nodes. Based on its promising in vitro and in vivo screening results, 12D6.2 (Fig. 1*G*) emerged as the lead ionizable lipid candidate for further optimization for circRNA delivery.

**DoE Optimization Identifies Key Parameters for Enhanced circRNA LNP Transfection.** Having identified 12D6.2 as a promising ionizable lipid for circRNA transfection, we next sought to improve its performance with formulation optimization. Previous studies have shown that the composition of LNP lipid components can strongly influence delivery ex vivo and in vivo and that the optimal LNP makeup can vary across cargo types (16, 18, 21, 27, 28). To refine our LNP composition for circRNA delivery, we therefore set out to investigate the influence of several factors on circRNA LNP performance. The first factor we investigated was the weight ratio of ionizable lipid to RNA cargo. Historically, siRNA LNP formulations have employed a 5:1 weight ratio, while many preclinical mRNA LNPs have used a ratio of 10:1 and more recently developed LNPs use a ratio as high as 20:1 (16, 29). As circRNA is a relatively large, covalently closed nucleic acid cargo, we opted to investigate the DOPC and SOPC helper lipids, previously employed for plasmid DNA (pDNA) delivery (18), in addition to the typical DSPC and DOPE helper lipids often employed for siRNA and mRNA delivery applications (16). We further investigated the influence of relative amount of both 12D6.2 ionizable lipid and helper lipid on LNP performance, as we reasoned that coordination with circRNA cargo could play an important role in improving circRNA encapsulation and delivery.

We used a Taguchi orthogonal DoE approach to reduce our initial design space of 256 distinct LNP formulations to a more manageable 16 formulations [Taguchi $L_{16}(4^4)$] (Fig. 2 *A* and *B*). We formulated these LNPs encapsulating NanoLuc circRNA ("library A") and, after physical characterization (*SI Appendix*, Table S2), again used them to transfect immune cell lines, comparing their transfection performance to the unoptimized 12D6.2 LNP based on typical mRNA LNP formulations (Fig. 2 *C*–*E*). This screen identified four LNP formulations with significantly greater NanoLuc transfection than the unoptimized 12D6.2 formulation in Jurkat cells (Fig. 2*D*) and two LNP formulations with significantly greater transfection in RAW 264.7 cells (Fig. 2*E*). We noted that the LNPs formulated with the SOPC helper lipid and greater lipid:RNA weight ratios generally performed best in all three cell lines (Fig. 2 *F*–*K*). This finding is consistent with the hit formulations identified, as the lead A14 LNP formulation is formulated with the SOPC helper lipid and at an ionizable lipid:RNA weight ratio of 20:1. Furthermore, these findings are consistent with the theory of ionizable lipid/helper lipid coordination with RNA cargo playing an important role in circRNA LNP performance.

Having identified favorable compositional parameters for circRNA encapsulation and delivery, we set out to further refine our LNP composition. We selected the SOPC helper lipid and 20:1

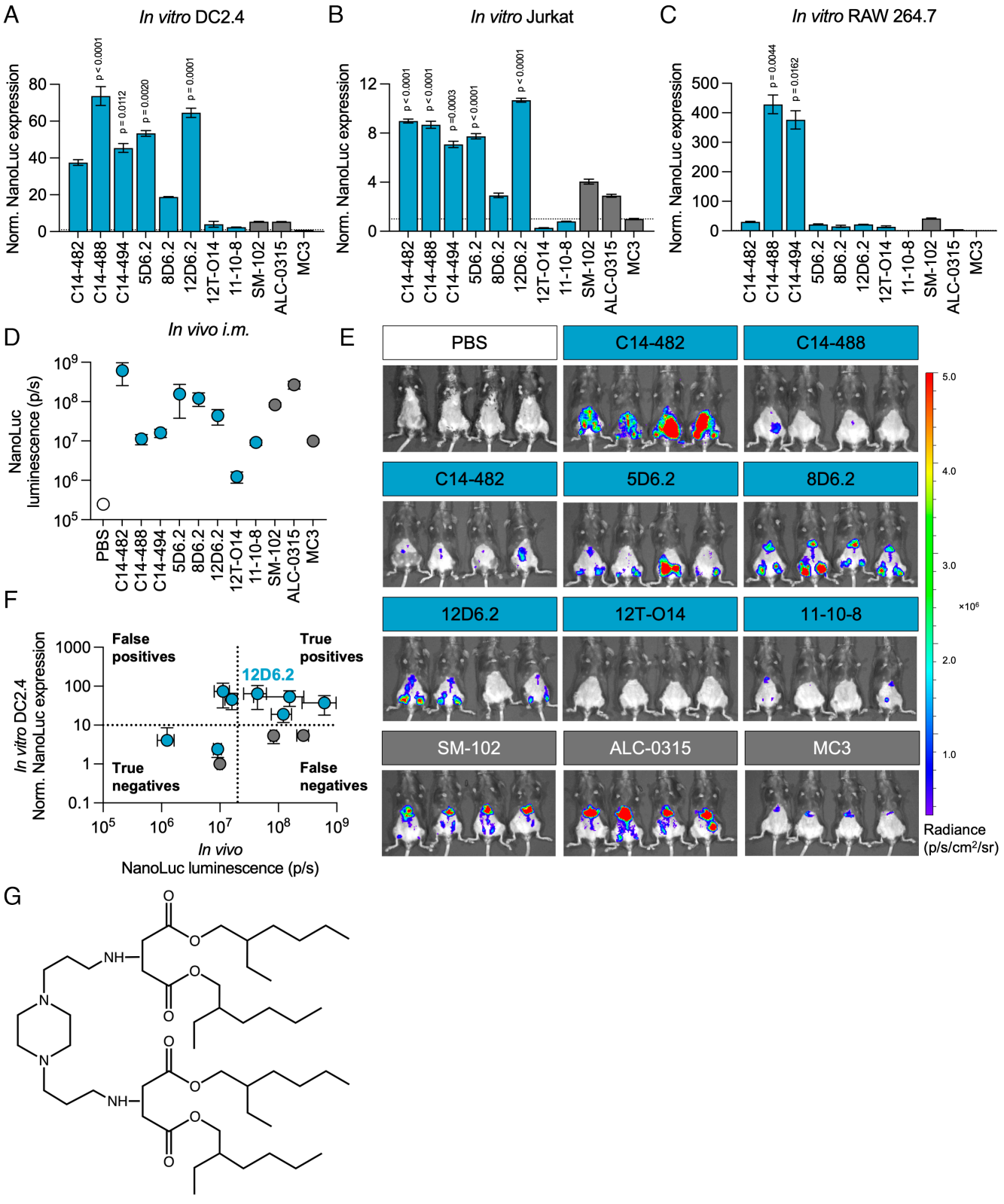


**Fig. 1.** LNPs formulated with the ionizable lipid 12D6.2 enable potent circRNA transfection in vitro and in vivo. (*A*–*C*) Relative NanoLuc expression in DC2.4 murine dendritic cells (DCs) (*A*), Jurkat human T cells (*B*), and RAW 264.7 murine macrophages (*C*) 24 h following transfection with unoptimized circRNA LNPs containing various ionizable lipids at a dose of 1 ng circRNA equivalent per 10,000 cells. Reported luminescence values are presented relative to DLin-MC3-DMA (MC3) circRNA LNPs. (*D* and *E*) Quantification (*D*) and bioluminescence images (*E*) of whole body NanoLuc expression in C57BL/6 mice 12 h following *i.m.* administration of unoptimized circRNA LNP formulations containing various ionizable lipids at a dose of 4 μg circRNA equivalent. (*F*) Comparison of in vitro and in vivo NanoLuc expression after treatment with unoptimized circRNA LNPs. (*G*) Chemical structure of lead ionizable lipid 12D6.2 for circRNA transfection. Data are presented as mean ± SEM (in vitro experiments: $n = 5$ independent biological replicates with 6 technical replicates each; in vivo experiments: $n = 4$ independent biological replicates). Nested two-sided, one-way analyses of variance (ANOVAs) with post hoc *t* tests using the Holm–Šídák correction for multiple comparisons were used for inferential analysis of LNP performance. Indicated *P* values summarize results from comparison to MC3 LNPs.

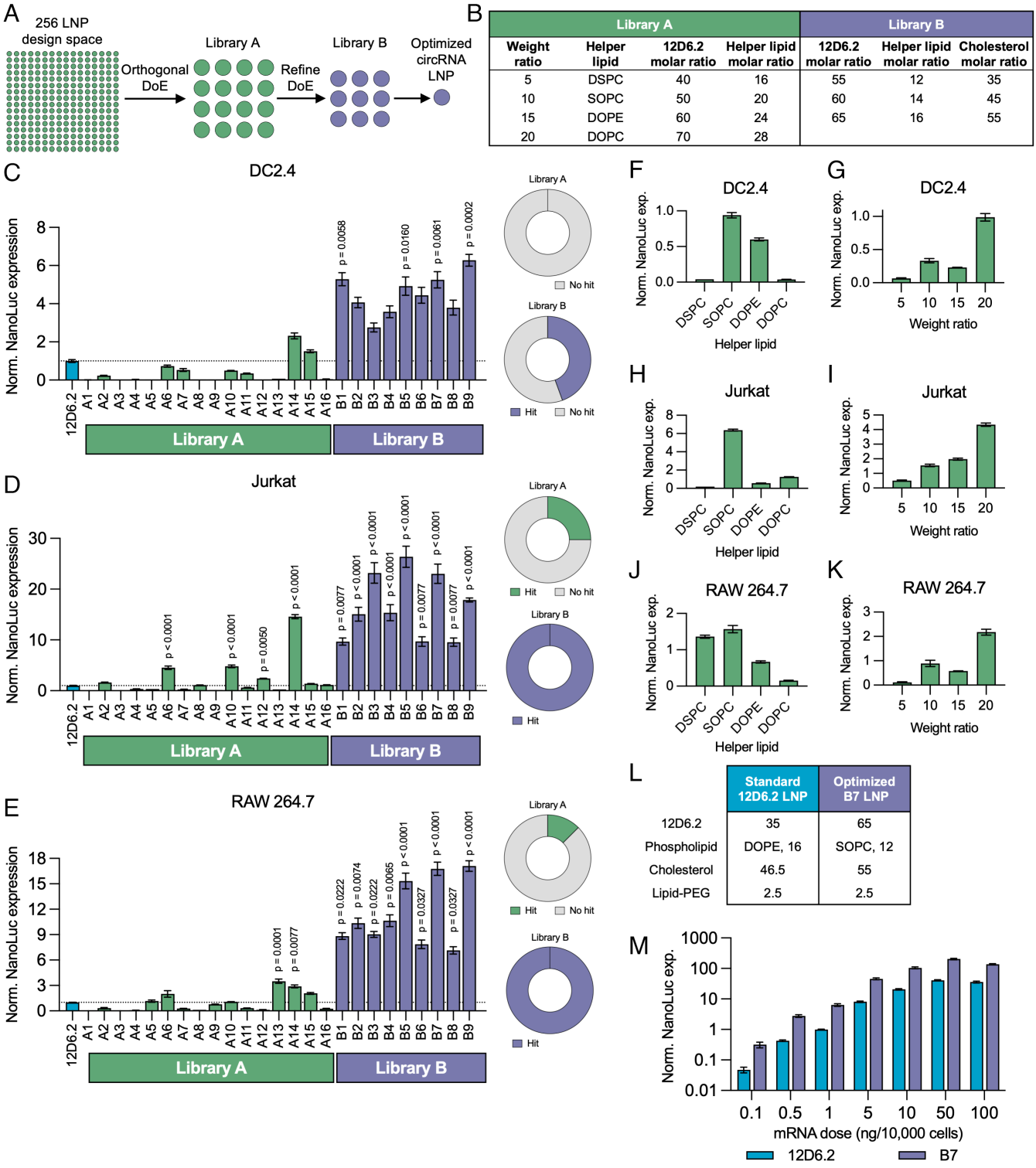


**Fig. 2.** Design-of-experiments (DoE) optimization of LNP lipid excipients enhances leukocyte circRNA transfection. (*A*) Schematic overview of the circRNA LNP optimization approach. A pair of sequential orthogonal DoE iterations was used to identify key parameters for circRNA encapsulation and transfection using LNPs. (*B*) Summary of lipid parameters investigated in orthogonal DoE refinement. Relative NanoLuc expression and library hit rate in DC2.4 murine DCs (*C*), Jurkat human T cells (*D*), and RAW 264.7 murine macrophages (*E*) 24 h following transfection with 12D6.2 LNPs of varying excipient composition at a dose of 1 ng circRNA equivalent per 10,000 cells. Blue bars (label: 12D6.2) and horizontal dashed lines represent the unoptimized formulation. Reported luminescence values are presented relative to the unoptimized formulation. (*F–K*) Analyses of the influence of helper lipid identity (*F*, *H*, and *J*) and ionizable lipid:circRNA weight ratio (*G*, *I*, and *K*) on relative leukocyte transfection in vitro, irrespective of other formulation parameters. (*L*) Summary of key differences in formulation parameters between standard and DoE-optimized (B7) 12D6.2 LNPs. (*M*) Dose–response data for 12D6.2 and B7 NanoLuc circRNA LNPs in DC2.4 cells. Data are presented as mean ± SEM ($n = 5$ independent biological replicates with 4 to 8 technical replicates each). Nested two-sided, one-way analyses of variance (ANOVAs) with post hoc *t* tests using the Holm–Šídák correction for multiple comparisons were used for inferential analysis of LNP performance. Indicated *P* values summarize results from comparison to unoptimized 12D6.2 circRNA LNPs.

weight ratio for all subsequent LNP formulations and opted to again vary ionizable lipid and helper lipid amount. In this optimization study, we also selected cholesterol content as a potentially interesting factor due to the role of cholesterol in lipid membrane rigidity and fusion (30). We again employed a DoE approach, formulating another 9 LNPs ("library B") to probe this refined

design space (Fig. 2 *A* and *B* and *SI Appendix*, Table S3). Evaluating these LNPs in immune cell lines using NanoLuc, we observed additional potent LNP formulations and a greater hit rate than in library A (Fig. 2 *C*–*E*). Strikingly, in Jurkat and RAW 264.7 cells, every formulation in library B exhibited significantly greater transfection than the mRNA-optimized base 12D6.2 LNP formulation (Fig. 2 *D* and *E*). Based on these results, we selected the B7 formulation, which demonstrated at least fivefold greater circRNA transfection than the unoptimized 12D6.2 LNP formulation in all immune cell types tested and outperformed the base formulation at all tested doses in DC2.4 cells, as our lead candidate for further evaluation (Fig. 2 *L* and *M*).

Interestingly, we observed that B7 circRNA LNPs, which demonstrated strong immune cell transfection, possessed atypical physicochemical properties for potent RNA LNPs. Namely, B7 circRNA LNPs were relatively large and demonstrated relatively low RNA entrapment efficiency (*SI Appendix*, Table S3). Future work should more closely evaluate the relationship between circRNA LNP physicochemical characteristics and immune transfection to determine whether optimal LNP properties for circRNA vaccines may differ from those of mRNA drugs and possible mechanisms responsible for these differences, which could potentially include factors such as differences in endocytic pathway, endosomal escape, or interactions with intracellular vesicles. It is also likely that these parameters exhibit synergistic effects with *e.g.*, ionizable lipid structure, as evidenced by preliminary data demonstrating differential effects of the B7 formulation when combined with clinical ionizable lipids (*SI Appendix*, Fig. S1). For instance, the substantial structural differences between the multibranched-tail 12D6.2 ionizable lipid (Fig. 1*G*) and the clinical SM-102, ALC-0315, and DLin-MC3-DMA ionizable lipids could play a role in the impact of the B7 formulation on circRNA transfection.

**Optimized circRNA LNP Formulations Accumulate in and Transfect Secondary Lymphoid Organs Following *i.m.* Administration.** RNA vaccines depend on the translation of antigen and its presentation in secondary lymphoid organs (11). While the precise mode of antigen production and transport is not fully understood, localization within the secondary lymphoid organs is crucial (31). We therefore endeavored to evaluate the in vivo translation and biodistribution profiles of our optimized circRNA LNP formulations. We formulated B7 LNPs encapsulating NanoLuc circRNA along with unoptimized 12D6.2 LNPs encapsulating either NanoLuc mRNA or NanoLuc circRNA. We tagged LNPs with the lipophilic fluorescent dye DiD, then administered LNPs *i.m.* to mice, collecting organs 12 h later for bioluminescence and fluorescence imaging. Using fluorescence imaging, we observed significant LNP accumulation in the inguinal and iliac lymph nodes (Fig. 3 *A*, *D*, and *E*) and apparent but not statistically significant accumulation in the spleen (Fig. 3*C*). We also observed marked accumulation of unoptimized 12D6.2 circRNA LNPs in the liver, which appeared to be reduced for our optimized B7 circRNA LNPs (Fig. 3 *A* and *B*).

Bioluminescence imaging of mouse organs showed apparent transfection in the liver, inguinal and iliac lymph nodes, and spleen (Fig. 3 *F*–*J*). Interestingly, optimized B7 circRNA LNPs displayed significantly greater liver transfection than either of the other LNP groups, despite demonstrating less accumulation. Optimized B7 circRNA LNPs demonstrated apparent increases in mean transfection compared to unoptimized 12D6.2 circRNA LNPs in the liver, spleen, and both types of lymph node (~4.7-fold increase in inguinal lymph nodes and ~4.4-fold increase in iliac lymph nodes), consistent with observed in vitro potency increases. While still lower than the expression induced by mRNA LNPs, this apparent partial rescue of protein production by LNP optimization is promising for circRNA vaccines, where strong and prolonged antigen production is desirable.

To better understand cellular interactions with our LNPs in secondary lymphoid organs, we further performed flow cytometric analysis of DiD fluorescence in cells isolated from the inguinal and iliac lymph nodes (Fig. 3 *K*–*R*) as well as from the spleen and peripheral blood (*SI Appendix*, Fig. S2). We observed significant and uniform accumulation of our optimized B7 circRNA LNPs in B cells, myeloid cells, and conventional DCs in both sets of lymph nodes, with roughly 10 to 15% DiD positivity across cell types in the inguinal lymph nodes (Fig. 3 *K*–*N*) and roughly 40% DiD positivity in the iliac lymph nodes (Fig. 3 *O*–*R*). Whereas unoptimized 12D6.2 mRNA/circRNA LNPs demonstrated significant accumulation within T cells in the inguinal lymph nodes, optimized B7 circRNA LNPs did not, suggesting preferential accumulation in APCs, a promising phenomenon for vaccine applications. Analysis of spleens and blood also demonstrated LNP accumulation in splenic leukocytes, though with somewhat less bias toward APC accumulation (*SI Appendix*, Fig. S2 *A*–*D*), as well as strong accumulation of circRNA LNPs within circulating APCs (*SI Appendix*, Fig. S2 *E*–*H*). This enhanced accumulation in APCs may be in part due to the size of B7 circRNA LNPs, which may promote phagocytosis in immune tissues. All told, these data suggest that optimized B7 circRNA LNPs can localize in APCs in secondary lymphoid organs following *i.m.* administration and that they induce strong transfection within these tissues.

**circRNA LNPs Induce Durable Transgene Expression.** A major advantage of circRNA over linear RNA species is its potential for long-lived gene expression. To assess the expression kinetics elicited by our optimized circRNA LNPs, we first evaluated in vitro NanoLuc expression in DC2.4 cells. We transfected cells with one of four LNP formulations: 1) clinical standard ALC-0315 LNPs encapsulating mRNA, 2) 12D6.2 LNPs encapsulating mRNA, 3) unoptimized 12D6.2 LNPs encapsulating circRNA, or 4) optimized B7 LNPs encapsulating circRNA. Daily for the next 10 d, we measured bioluminescence signal using a plate reader (Fig. 4*A*). Strikingly, both circRNA LNPs tested demonstrated substantially greater transgene expression than either mRNA LNP formulation, even at earlier timepoints when cap-dependent mRNA translation—which is rapid-onset and would be expected to continue until substantial RNase-mediated cargo degradation occurs—would be expected to outpace relatively slow cap-independent circRNA translation (32). The optimized B7 circRNA LNP formulation demonstrated remarkable transgene expression, with an area-under-the-curve (AUC) analysis identifying a nearly fourfold increase in cumulative translation compared to the unoptimized 12D6.2 circRNA formulation and an over 20-fold increase in cumulative expression compared to the 12D6.2 mRNA formulation (Fig. 4*B*). We also assessed the relative persistence of gene expression by comparing bioluminescence measurements to the performance of each group on the first day after transfection, observing greater expression durability in both circRNA treatment groups than in either mRNA treatment group, as expected (Fig. 4*C*).

As optimized B7 circRNA LNPs demonstrated favorable in vitro expression kinetics, we next set out to evaluate the in vivo expression kinetics of our LNP formulations. We administered mRNA or circRNA LNPs *i.m.* to mice and performed whole-body

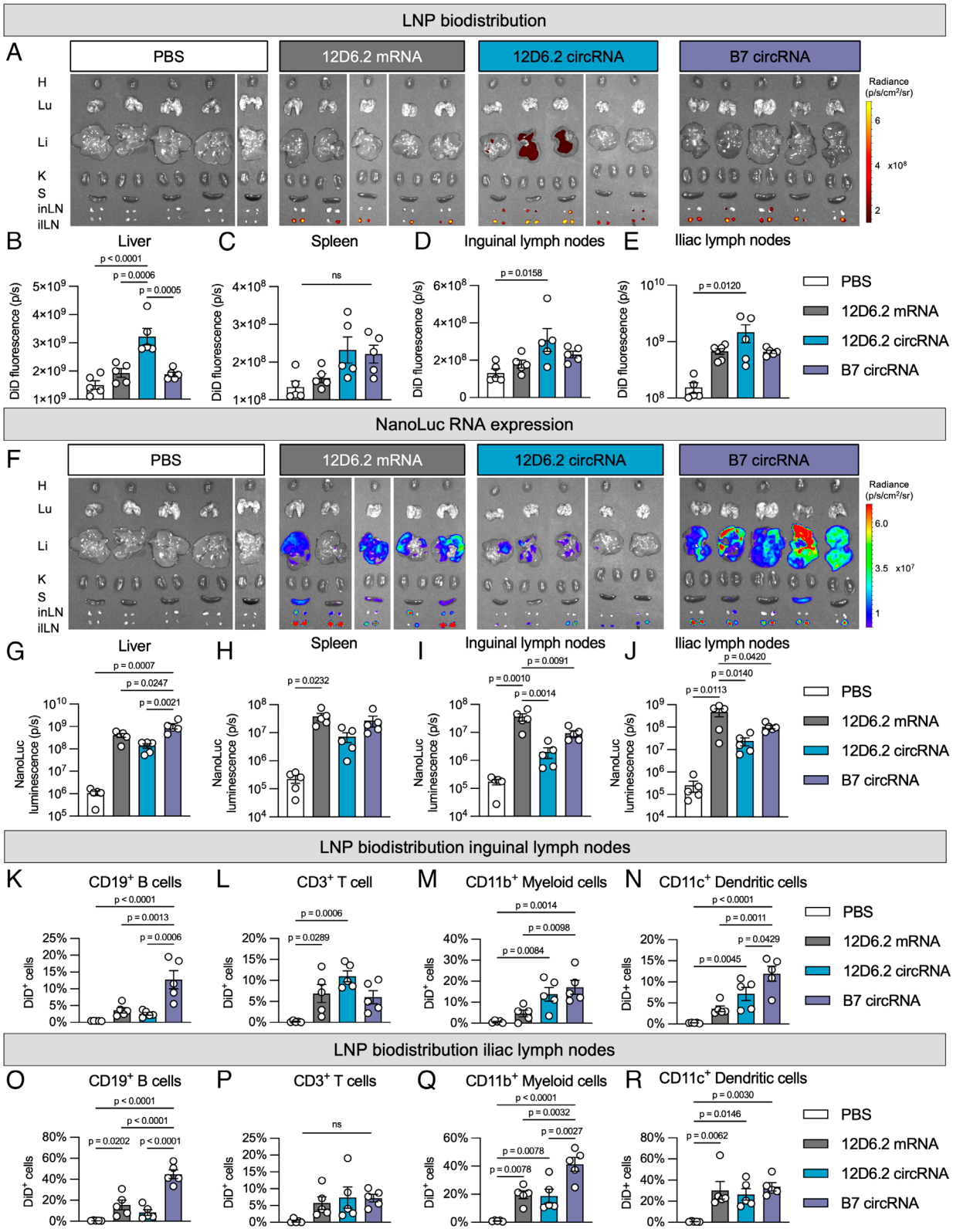


**Fig. 3.** Optimized circRNA LNPs accumulate in and transfect secondary lymphoid tissues following *i.m.* administration. (*A–E*) Images (*A*) and quantification (*B–E*) of fluorescence signal from DiD-tagged LNPs 12 h following *i.m.* administration in C57BL/6 mice at a dose of 4 μg circRNA equivalent. Mice were treated with phosphate-buffered saline (PBS), 12D6.2 LNPs containing mRNA (12D6.2 mRNA), unoptimized 12D6.2 LNPs containing circRNA (12D6.2 circRNA), or optimized 12D6.2 LNPs containing circRNA (B7 circRNA). (*F–J*) Images (*F*) and quantification (*G–J*) of luminescence signal 12 h following *i.m.* administration of LNPs containing NanoLuc RNA to C57BL/6 mice. IVIS images are separated by white space to indicate multiple original sources as images were taken at different times or data were excluded due to failed injections. (*K–N*) Flow cytometric analysis of accumulation of DiD-tagged LNPs within $CD19^+$ B cells (*K*), $CD3^+$ T cells (*L*), $CD11b^+$ myeloid cells (*M*), and $CD11c^+$ DCs (*N*) in the inguinal lymph nodes 12 h following *i.m.* administration. (*O–R*) Flow cytometric analysis of accumulation of DiD-tagged LNPs within $CD19^+$ B cells (*O*), $CD3^+$ T cells (*P*), $CD11b^+$ myeloid cells (*Q*), and $CD11c^+$ DCs (*R*) in the iliac lymph nodes 12 h following *i.m.* administration. Data are presented as mean ± SEM ($n = 5$ independent biological replicates). Two-sided, one-way analyses of variance (ANOVAs) with post hoc *t* tests using the Holm–Šídák correction for multiple comparisons were used for inferential analysis of LNP performance.

bioluminescence measurements over the course of 28 d (Fig. 4 *D* and *G–J*). Here, we observed that mRNA LNPs conferred generally higher NanoLuc expression levels, contrary to in vitro results (Fig. 4*D*). Notably, however, while 12D6.2 mRNA LNPs demonstrated roughly order-of-magnitude greater cumulative gene expression than unoptimized 12D6.2 circRNA LNPs throughout the study, we observed gene expression characteristics more comparable to mRNA LNPs with optimized circRNA LNPs, achieving a 2.6-fold improvement in NanoLuc expression compared to unoptimized circRNA LNPs (Fig. 4*E*). This finding is consistent with prior transfection data suggesting that LNP optimization can partially rescue decreased protein production from circRNA cargo relative to mRNA (Fig. 3 *F–J*). Moreover, we again observed an apparently slower decay of luminescence signal for circRNA LNPs relative to mRNA LNPs containing the same ionizable lipid, particularly at short time points (up to seven days post-transfection) (Fig. 4 *F* and *G*). All told, these data suggest strong durability of transgene expression lasting up to 28 d after administration, with circRNA LNP optimization substantially bolstering in vivo transgene expression.

**circRNA LNPs Promote In Vivo DC Maturation in Draining Inguinal Lymph Nodes.** Having demonstrated the transfection potential of our circRNA LNP formulations in secondary lymphoid organs and strong expression kinetics, we next sought to evaluate LNP immune interactions. We encapsulated RNA encoding the spike (S) glycoprotein of SARS-CoV-2 variant B.1.617.2 (Delta) in LNPs and delivered them via *i.m.* administration to mice. The following day, we isolated iliac and inguinal lymph nodes and performed flow cytometric analysis of lymph node DCs, evaluating expression of the DC maturation markers CD80 and CD86 (Fig. 5*A*). In the iliac lymph nodes, we observed a significant increase in CD86 expression by DCs following treatment with ALC-0315 mRNA LNPs but no other significant differences (Fig. 5 *D–E*). However, in the inguinal lymph nodes, we observed significant increases in both CD80 and CD86 expression by DCs following treatment with B7 circRNA LNPs (Fig. 5 *B* and *C*). These increases were comparable to those observed for clinical standard ALC-0315 mRNA LNPs, and CD86 expression was significantly greater following treatment with optimized B7 circRNA LNPs than after 12D6.2 mRNA LNP treatment. These results indicate that B7 circRNA LNPs can promote DC maturation, suggestive of effective self-adjuvanticity, an attractive property for vaccine applications.

**circRNA LNP Vaccine Against SARS-CoV-2 Produces Strong Cellular and Humoral Immune Responses.** As B7 circRNA LNPs had demonstrated their potential for immune stimulation, we finally sought to explore their use for vaccination against infectious diseases. We formulated LNPs encapsulating mRNA or circRNA encoding SARS-CoV-2 B.1.617.2 (Delta) S glycoprotein, immunizing mice on days 0 and 21 with one of three LNP formulations: 1) ALC-0315 mRNA LNPs, 2) 12D6.2 mRNA LNPs, or 3) optimized B7 circRNA LNPs. To investigate the potential for dose sparing, we also tested a single administration of optimized B7 circRNA LNPs on day 0, reasoning that prolonged antigen expression following circRNA transfection might obviate the need for a second administration. On day 35, mice were euthanized according to our approved IACUC protocol and we assessed SARS-CoV-2 receptor binding domain (RBD)-specific T cell responses and serum levels of anti-RBD antibody as measures of cellular and humoral immunity, respectively (Fig. 6*A*). All vaccination schemes produced high levels of anti-RBD IgG (Fig. 6 *B–D*); however, the single-administration circRNA LNP vaccination approach yielded significantly lower total IgG serum levels than the prime-boost circRNA vaccination scheme (Fig. 6*D*). Nonetheless, optimized B7 circRNA LNPs engendered comparable levels of anti-RBD IgG2c and IgG1 to clinical standard ALC-0315 mRNA LNPs (Fig. 6 *C* and *D*) and apparently higher levels of total anti-RBD IgG than either mRNA LNP tested, demonstrating roughly 3.8-fold greater total IgG titers than ALC-0315 mRNA LNPs and roughly fivefold greater titers than 12D6.2 mRNA LNPs (Fig. 6*B*). Moreover, all LNP treatments following a prime-boost immunization scheme induced a $T_h1$-skewed response as reflected by IgG2c/IgG1 ratio (Fig. 6*E*), favorable for strong immune protection that avoids disease enhancement (32). In sum, optimized B7 circRNA LNPs appeared to induce a stronger humoral immune response than ALC-0315 mRNA LNPs, demonstrating the promise of this platform for circRNA vaccination.

We next evaluated cellular immune responses to LNP vaccination by stimulating splenocytes from vaccinated mice with SARS-CoV-2 B.1.617.2 (Delta) RBD peptide. We performed intracellular staining to facilitate flow cytometric analysis of cytokine production. Among $CD4^+$ T cells, we broadly observed comparable levels of $T_h1$-associated cytokines (Fig. 6 *F–H*) following vaccination with ALC-0315 mRNA LNPs or with optimized B7 circRNA LNPs, either with or without the boost dose; however, we generally observed similar or lower levels of $T_h2$-associated cytokines (Fig. 6 *I–K*) following vaccination with optimized B7 circRNA LNPs compared to ALC-0315 mRNA LNPs, again suggestive of a $T_h1$-shifted immune response. We also evaluated cytokine production by $CD8^+$ T cells, observing similar or lower levels of interferon (IFN)-γ (Fig. 6*L*), interleukin (IL)-2 (Fig. 6*M*), and tumor necrosis factor (TNF) (Fig. 6*N*) in groups receiving optimized B7 circRNA LNPs compared to those receiving mRNA LNPs. We also observed similar or higher rates of $CD8^+IFN\text{-}\gamma^+CD107a^+$ T cells in groups receiving optimized B7 circRNA LNPs compared to mRNA LNPs (Fig. 6*O*). Moreover, we observed increases in polyfunctional T cell frequency following RNA LNP vaccination (*SI Appendix*, Fig. S3). Interestingly, cytokine production was generally higher in groups receiving only a single administration of circRNA LNPs compared to those receiving a boost dose. Future studies should closely investigate the kinetics of circRNA vaccine immune responses to establish optimized prime-boost regimens for vaccination given the durable antigen production potential of circRNA. Together with serum antibody analysis, these data suggest a $T_h1$-biased cellular immune response to vaccination with circRNA LNPs with comparable or superior levels of humoral immunity to clinical-standard ALC-0315 mRNA LNPs.

## Discussion

circRNA is an attractive emerging RNA cargo for use in therapeutics and vaccines due to its stability in biological environments, arising from its covalently closed structure. However, surprisingly little investigation has been performed to optimize circRNA delivery in vivo, with most protein-coding circRNA delivery studies simply repurposing mRNA LNP formulations (7, 13–15). Here, we systematically optimized LNP formulation parameters to engineer circRNA LNPs for cargo delivery to immune cells in vivo.

We first identified an ionizable lipid, 12D6.2, with promising circRNA encapsulation and delivery characteristics using a combination of in vitro and in vivo screening (Fig. 1). This ionizable lipid is easily and rapidly synthesized using commercially available reagents (23). Excitingly, unoptimized 12D6.2 circRNA LNPs mediate circRNA transfection in immune cell lines and induce greater transgene expression than clinical standard LNP

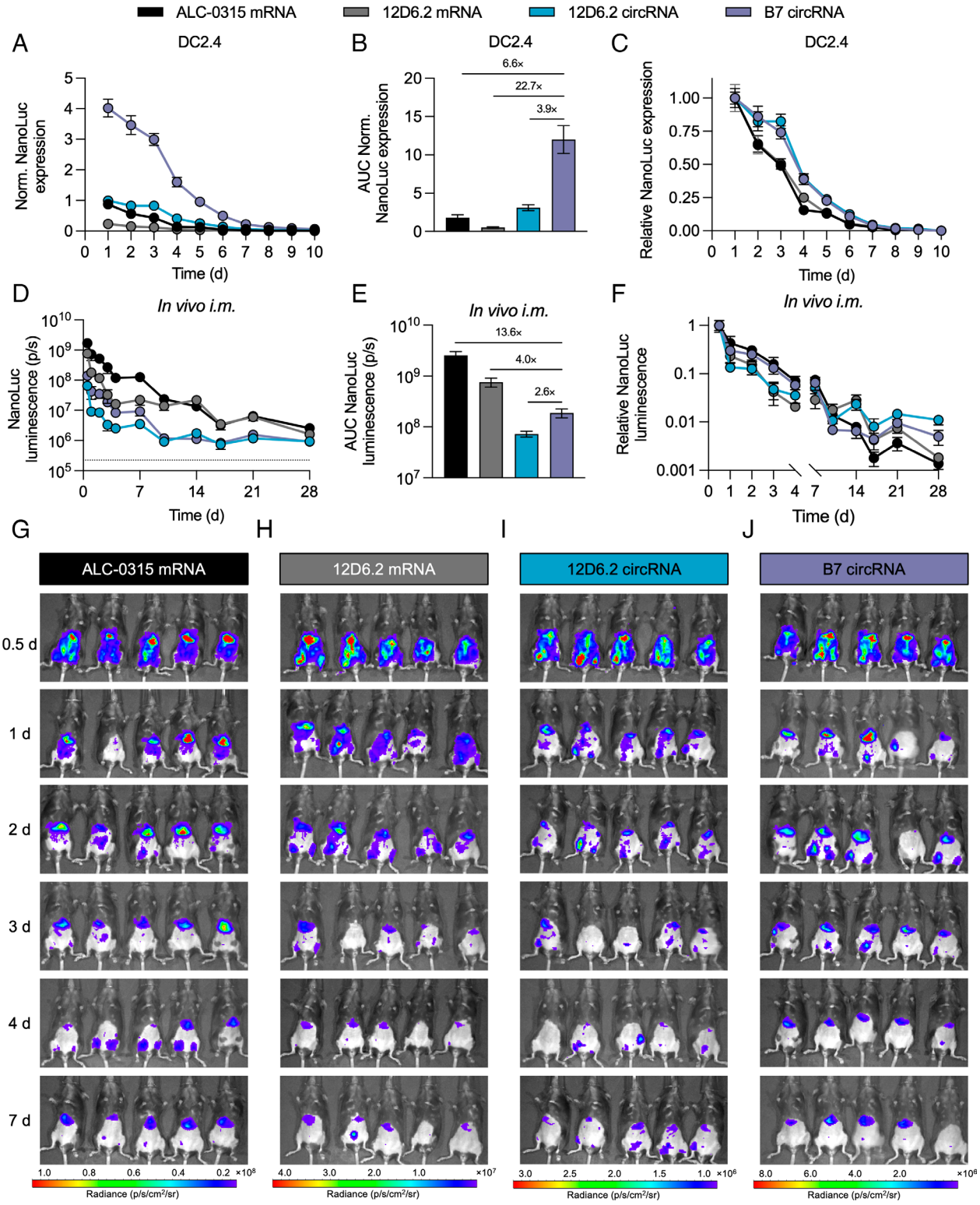


**Fig. 4.** circRNA LNP formulation optimization drives durable protein translation in vitro and in vivo. (*A*) Relative NanoLuciferase (NanoLuc) expression by DC2.4 murine DCs following treatment with mRNA or circRNA LNPs at a dose of 10 ng circRNA equivalent per 10,000 cells. Clinical standard ALC-0315 LNPs encapsulating NanoLuc mRNA (ALC-0315 mRNA), 12D6.2 LNPs encapsulating NanoLuc mRNA (12D6.2 mRNA), unoptimized 12D6.2 LNPs encapsulating NanoLuc circRNA (12D6.2 circRNA), and optimized 12D6.2 LNPs encapsulating NanoLuc circRNA (B7 circRNA) were used as treatment groups. Luminescence measurements are presented relative to ALC-0315 mRNA LNPs 24 h post-transfection. (*B*) Area-under-the-curve (AUC) analysis of cumulative NanoLuc expression in (*A*). (*C*) Relative persistence of RNA-induced NanoLuc expression from (*A*). Data are presented relative to each treatment's luminescence signal 24 h after transfection to visualize signal decay profiles. (*D*) Whole-body luminescence in C57BL/6 mice following *i.m.* administration of NanoLuc RNA LNPs at a dose of 2 μg circRNA equivalent. The dashed horizontal line indicates average background value from untreated mice over the 28-day study. (*E*) AUC analysis of cumulative NanoLuc expression in (*D*). (*F*) Relative persistence of RNA-induced NanoLuc expression from (*D*). Data are presented relative to the luminescence signal of each treatment group 12 h after treatment to visualize signal decay profiles. (*G–J*) Bioluminescence images following treatment with ALC-0315 LNPs encapsulating NanoLuc mRNA (*G*), 12D6.2 LNPs encapsulating NanoLuc mRNA (*H*), unoptimized 12D6.2 LNPs encapsulating NanoLuc circRNA (*I*), or optimized 12D6.2 LNPs encapsulating NanoLuc circRNA (*J*). Data are presented as mean ± SEM ($n = 5$ independent biological replicates). Two-sided, one-way analyses of variance (ANOVAs) with post hoc *t* tests using the Holm–Šídák correction for multiple comparisons were used for inferential analysis of LNP performance.

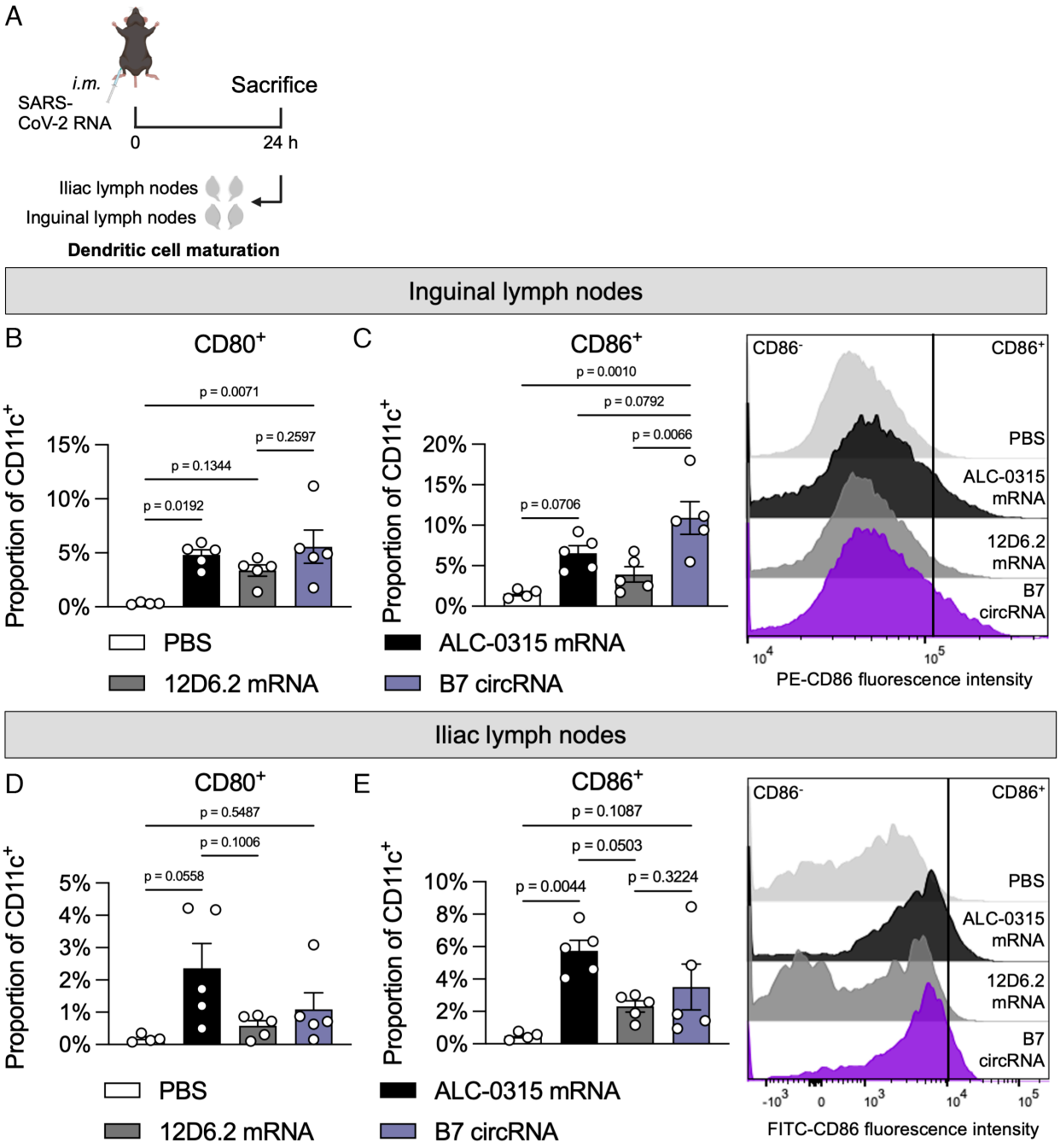


**Fig. 5.** Optimized circRNA LNPs trigger DC maturation following *i.m.* vaccination against SARS-CoV-2. (*A*) Schematic overview of DC maturation study. Mice were injected with LNPs containing RNA encoding the SARS-CoV-2 B.1.617.2 Spike (S) protein at a dose of 4 μg of circRNA equivalent. 24 h later, mice were euthanized according to the approved procedure by the University of Pennsylvania's Institutional Animal Care and Use Committee (IACUC), and iliac and inguinal lymph nodes were collected for analysis of DC maturation. (*B*–*E*) Flow cytometric analysis of DC maturation markers CD80 (*B* and *D*) and CD86 (*C* and *E*) in DCs isolated from the inguinal (*B* and *C*) or iliac (*D* and *E*) lymph nodes following treatment with spike RNA LNPs. Data are presented as mean ± SEM ($n = 5$ independent biological replicates). Two-sided, one-way analyses of variance (ANOVAs) with post hoc *t* tests using the Holm–Šídák correction for multiple comparisons were used for inferential analysis of DC maturation.

formulations in vivo. The strong transfection characteristics of unoptimized LNPs made with this ionizable lipid demonstrate the suitability of 12D6.2 LNPs for circRNA delivery even without further formulation development. This prowess, combined with ease of synthesis, makes 12D6.2 a promising lipid for future investigations into circRNA delivery. As we observed promising transfection following *i.v.* administration, future investigations into systemic administration of B7 or other 12D6.2 LNPs encapsulating circRNA could lead to interesting therapeutic developments.

We further optimized LNP formulation parameters for circRNA encapsulation and delivery through a nested DoE approach (Fig. 2*A*). This iterative refinement granted substantial insight into key formulation parameters for circRNA encapsulation and delivery with LNPs. Notably, circRNA LNPs benefited from an increased ratio of ionizable lipid to RNA payload and a greater mole fraction of ionizable lipid, perhaps due to interactions with polar RNA cargo. Interestingly, incorporation of the SOPC helper lipid, previously employed for pDNA delivery, also greatly bolstered LNP performance. While future work should investigate cargo

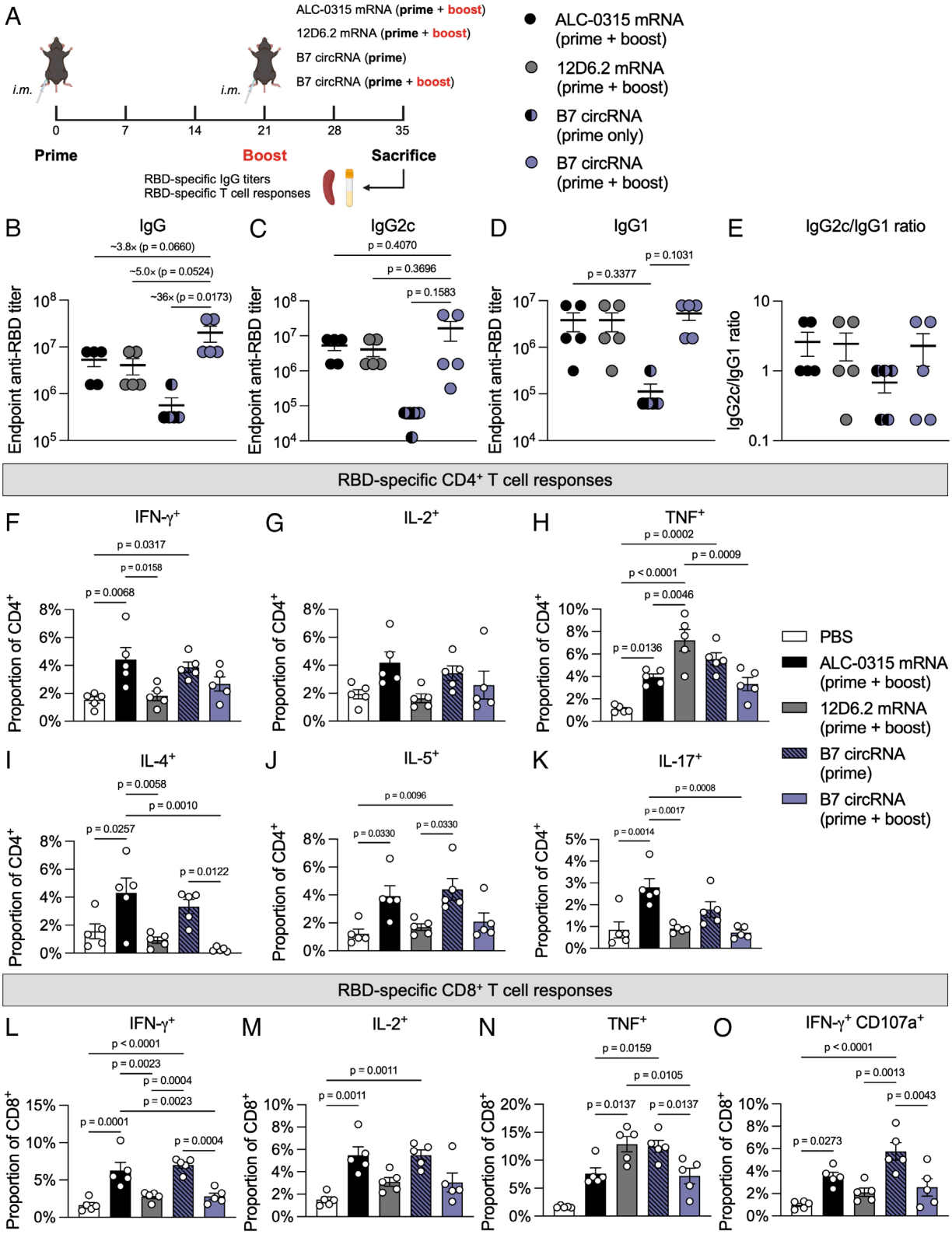


**Fig. 6.** Optimized circRNA LNP formulations induce a specific inflammatory response against SARS-CoV-2 antigen. (*A*) Schematic overview of vaccination study. Mice were immunized on day 0 (prime) and/or day 21 (boost) with clinical standard ALC-0315 LNPs encapsulating mRNA encoding SARS-CoV-2 B.1.617.2 Spike (S) protein (ALC-0315 mRNA), 12D6.2 LNPs encapsulating S mRNA (12D6.2 mRNA), or optimized 12D6.2 LNPs encapsulating S circRNA (B7 circRNA) at a dose of 4 μg circRNA equivalent. Sera and spleens were collected on day 35 to assess anti-S receptor binding domain (RBD) antibody levels and RBD-specific T cell responses. (*B–D*) RBD-specific reciprocal endpoint IgG (*B*), IgG2c (*C*), and IgG1 (*D*) titers following immunization. (*E*) Ratio of RBD-specific reciprocal endpoint IgG2c/IgG1 titers. Greater values suggest a more $T_h1$-skewed response. (*F–O*) Flow cytometric analysis of RBD-specific $CD4^+$ helper (*F–K*) and $CD8^+$ cytotoxic (*L–O*) T cell response following ex vivo stimulation of splenocytes from vaccinated mice with an RBD peptide pool. Intracellular staining was performed to assess the proportion of T cells producing cytolytic marker CD107, $T_h1$ cytokines [interferon (IFN)-γ, interleukin (IL)-2, tumor necrosis factor (TNF)], $T_h2$ cytokines (IL-4, IL-5), and $T_h17$ cytokine (IL-17) in response to RBD stimulation. Data are presented as mean ± SEM ($n = 5$ independent biological replicates). Two-sided, one-way analyses of variance (ANOVAs) with post hoc *t* tests using the Holm–Šídák correction for multiple comparisons were used for inferential analysis of antibody titers and cytokine production.

packing into circRNA LNPs in greater detail, these findings suggest potential lipid–cargo interactions and key parameters for the effective encapsulation and delivery of this emerging RNA cargo.

To explore the potential of our engineered circRNA LNPs for in vivo delivery, we evaluated the biodistribution and transfection profile of optimized B7 circRNA LNPs following *i.m.* administration (Fig. 3). We observed preferential accumulation of these optimized circRNA LNPs in APCs in secondary lymphoid organs and strong transfection of these tissues. Interestingly, we observed generally stronger LNP performance in the iliac lymph nodes than in the inguinal lymph nodes following intramuscular administration into the hindlimb. Though studies commonly interrogate the inguinal lymph nodes, recent work has identified the iliac lymph nodes as organs of interest following vaccination, and future studies may wish to favor the analysis of these lymph nodes (31, 33, 34). We also performed a preliminary evaluation of our circRNA LNPs following *i.v.* administration, observing transfection of both the liver and secondary lymphoid tissues (*SI Appendix*, Fig. S4). While DoE optimization improved RNA transfection and LNP accumulation in APCs following *i.m.* administration, interestingly the unoptimized 12D6.2 circRNA LNP and the DoE optimized B7 circRNA LNP induced comparable NanoLuc expression upon *i.v.* administration. These results are consistent with a previous report by our group that utilized high-throughput in vivo screening to demonstrate a strong influence of excipient composition on LNP performance upon *i.m.* administration but not *i.v.* administration (22).

In addition to biodistribution, we further evaluated the expression kinetics induced by our circRNA LNPs, demonstrating strong and durable transgene expression, as expected (Fig. 4). Notably, while we demonstrated partial rescue of transgene expression through circRNA LNP optimization, protein production levels were generally lower than those engendered by mRNA LNPs. This disparity between mRNA and circRNA expression has been explored previously (17), and as RNA engineering efforts continue to improve the magnitude of cap-independent translation, we expect circRNA to emerge as a candidate for applications requiring prolonged protein production.

The potent and durable transgene expression in secondary lymphoid organs induced by our optimized circRNA LNPs led us to pursue their application to prophylactic vaccination. We first confirmed the adjuvanticity of our circRNA LNPs by evaluating DC maturation in the draining lymph nodes (Fig. 5), demonstrating substantial increases in maturation markers. With this result in hand, we immunized mice against SARS-CoV-2 B.1.617.2 (Delta) and evaluated the effects of vaccination with optimized circRNA LNPs (Fig. 6). Here, we observed strong humoral immunity with a $T_h1$-biased cellular immune response, both indicative of successful vaccination with induction of favorable immune responses. These findings ultimately confirm the promise of our optimized circRNA LNP platform for direct modulation of the immune system in vivo, particularly for vaccination. Because of the improved manufacturability and stability of circRNA cargo compared to mRNA, vaccines based on this technology could be quite attractive for use in developing countries and locations with poor access to cold chain storage to protect against both emerging SARS-CoV-2 variants and other pathogens. We have collected preliminary data on shelf stability of circRNA LNPs that suggests circRNA LNPs generally demonstrate greater retention of transfection ability over time than their mRNA counterparts (*SI Appendix*, Fig. S5)—an exciting finding for vaccine deployment in the developing world that should be further evaluated in future studies.

In summary, we develop optimized LNP formulations for the encapsulation and intracellular delivery of circRNA cargo, demonstrating substantial improvements compared to mRNA LNP formulations and identifying key design considerations for circRNA LNP drug products. We further demonstrate favorable in vivo accumulation of administered circRNA LNPs in APCs in the secondary lymphoid organs along with strong transfection of lymphoid tissues. We immunize mice with optimized LNPs encapsulating SARS-CoV-2 B.1.617.2 (Delta) Spike circRNA and provoke strong antigen-specific cellular and humoral responses, demonstrating the suitability of this emerging cargo and delivery platform for vaccination against infectious disease.

## Methods

A detailed version of the experimental methods used in this article is provided in the *SI Appendix*. In brief, linear and circular RNA were synthesized with T7 RNA polymerase and used to formulate LNPs via microfluidic mixing of an aqueous RNA phase and an ethanol phase containing lipid excipients. After formulation, LNP size, polydispersity, encapsulation efficiency, and RNA concentration were characterized. In vitro experiments were performed in immortalized Jurkat human T cells, RAW 264.7 murine macrophages, and DC2.4 murine DCs; cells were treated with RNA LNPs and NanoLuc bioluminescence was measured using a plate reader via the addition of Nano-Glo detection reagent. For in vivo assays, female C57BL6 mice were treated with RNA LNPs via *i.m.* or *i.v.* administration and bioluminescence and fluorescence imaging was performed using an in vivo imaging system. In some experiments, iliac lymph nodes, inguinal lymph nodes, spleens, and blood were collected for further analysis via flow cytometry. Finally, mice were vaccinated with RNA encoding SARS-CoV-2 B.1.617.2 Spike (S) protein on a prime/boost schedule at a three-week interval, and anti-RBD antibody titers were assessed using ELISAs. Ordinary or nested two-sided, one-way analyses of variance (ANOVAs) with post hoc Student's *t* tests with the Holm–Šídák correction for multiple comparisons were employed for comparisons across multiple groups.

**Data, Materials, and Software Availability.** All study data are included in the article and/or *SI Appendix*.

**ACKNOWLEDGMENTS.** M.J.M. acknowledges funding support from a NSF CAREER Award (CBET-2145491), the Burroughs Wellcome Fund Career Award at the Scientific Interface, and the American Cancer Society (RGS-22-1122-01-ET). K.L.S., A.G.H., H.C.S., A.S.T., and H.C.S. were supported by NSF Graduate Research Fellowships (award 1845298). This work is supported by Wellcome Leap as part of the R3 Program and by the HHP IAF-PP Progamme (H22J1a0050), Singapore. Some data for this manuscript were generated in the Penn Cytomics and Cell Sorting Shared Resource Laboratory at the University of Pennsylvania (RRid:SCR_022376), partially supported by a National Cancer Institute (NCI) grant at the Abramson Cancer Center (P30 016520).

Author affiliations: [a]Department of Bioengineering, University of Pennsylvania, Philadelphia, PA 19104; [b]Genome Institute of Singapore, Agency for Science, Technology, and Research (A*STAR), Singapore 138672, Singapore; [c]Penn Institute for RNA Innovation, University of Pennsylvania, Philadelphia, PA 19104; [d]Abramson Cancer Center, Perelman School of Medicine, University of Pennsylvania, Philadelphia, PA 19104; [e]Institute for Immunology, Perelman School of Medicine, University of Pennsylvania, Philadelphia, PA 19104; [f]Cardiovascular Institute, Perelman School of Medicine, University of Pennsylvania, Philadelphia, PA 19104; [g]Institute for Regenerative Medicine, Perelman School of Medicine, University of Pennsylvania, Philadelphia, PA 19104; [h]Center for Cellular Immunotherapies, Perelman School of Medicine, University of Pennsylvania, Philadelphia, PA 19104; and [i]Center for Precision Engineering for Health, University of Pennsylvania, Philadelphia, PA 19104

1. F. P. Polack *et al.*, Safety and efficacy of the BNT162b2 mRNA Covid-19 vaccine. *N. Engl. J. Med.* **383**, 2603–2615 (2020).
2. L. R. Baden *et al.*, Efficacy and safety of the mRNA-1273 SARS-CoV-2 vaccine. *N. Engl. J. Med.* **384**, 403–416 (2021).
3. A. G. Lokras, T. R. Bobak, S. S. Baghel, F. Sebastiani, C. Foged, Advances in the design and delivery of RNA vaccines for infectious diseases. *Adv. Drug Deliv. Rev.* **213**, 115419 (2024).
4. C. P. Arevalo *et al.*, A multivalent nucleoside-modified mRNA vaccine against all known influenza virus subtypes. *Science* **378**, 899–904 (2022).

5. H. Parhiz, E. N. Atochina-Vasserman, D. Weissman, mRNA-based therapeutics: Looking beyond COVID-19 vaccines. *Lancet* **403**, 1192–1204 (2024).
6. R. A. Wesselhoeft, P. S. Kowalski, D. G. Anderson, Engineering circular RNA for potent and stable translation in eukaryotic cells. *Nat. Commun.* **9**, 2629 (2018).
7. R. A. Wesselhoeft *et al.*, RNA circularization diminishes immunogenicity and can extend translation duration in vivo. *Mol. Cell* **74**, 508–520.e4 (2019).
8. K. L. Swingle, A. G. Hamilton, M. J. Mitchell, Lipid nanoparticle-mediated delivery of mRNA therapeutics and vaccines. *Trends Mol. Med.* **27**, 616–617 (2021).
9. A. G. Hamilton, K. L. Swingle, M. J. Mitchell, Biotechnology: Overcoming biological barriers to nucleic acid delivery using lipid nanoparticles. *PLOS Biol.* **21**, e3002105 (2023).
10. K. Karikó *et al.*, Incorporation of pseudouridine into mRNA yields superior nonimmunogenic vector with increased translational capacity and biological stability. *Mol. Ther. J. Am. Soc. Gene Ther.* **16**, 1833–1840 (2008).
11. N. Pardi, M. J. Hogan, F. W. Porter, D. Weissman, mRNA vaccines–a new era in vaccinology. *Nat. Rev. Drug Discov.* **17**, 261 (2018).
12. T. Loan Young, K. Chang Wang, A. James Varley, B. Li, Clinical delivery of circular RNA: Lessons learned from RNA drug development. *Adv. Drug Deliv. Rev.* **197**, 114826 (2023).
13. Z. Feng *et al.*, Engineered GSDMD in vitro transcribed circRNA targeting mitochondrial inner membrane cardiolipin for the ablation of EIF4G2+/PTBP1+ panadenocarcinoma. *Nat. Cancer* **5**, 30–46 (2023).
14. S. Xu *et al.*, Tumor-tailored ionizable lipid nanoparticles facilitate IL-12 circular RNA delivery for enhanced lung cancer immunotherapy. *Adv. Mater.* **36**, 2400307 (2024).
15. J. Liu *et al.*, A single dose of VEGF-A circular RNA sustains in situ long-term expression of protein to accelerate diabetic wound healing. *J. Controlled Release* **373**, 319–335 (2024).
16. K. J. Kauffman *et al.*, Optimization of lipid nanoparticle formulations for mRNA delivery in vivo with fractional factorial and definitive screening designs. *Nano Lett.* **15**, 7300–7306 (2015).
17. R. Chen *et al.*, Engineering circular RNA for enhanced protein production. *Nat. Biotechnol.* **41**, 262–272 (2022), 10.1038/s41587-022-01393-0.
18. J. A. Kulkarni *et al.*, Design of lipid nanoparticles for in vitro and in vivo delivery of plasmid DNA. *Nanomed. Nanotechnol. Biol. Med.* **13**, 1377–1387 (2017).
19. M. M. Billingsley *et al.*, Ionizable lipid nanoparticle-mediated mRNA delivery for human CAR T cell engineering. *Nano Lett.* **20**, 1578–1589 (2020).
20. A. J. Mukalel *et al.*, Oxidized mRNA lipid nanoparticles for in situ chimeric antigen receptor monocyte engineering. *Adv. Funct. Mater.* **34**, 2312038 (2024).
21. A. G. Hamilton *et al.*, Ionizable lipid nanoparticles with integrated immune checkpoint inhibition for mRNA CAR T cell engineering. *Adv. Healthc. Mater.* **12**, 2301515 (2023).
22. A. G. Hamilton *et al.*, High-throughput in vivo screening identifies differential influences on mRNA lipid nanoparticle immune cell delivery by administration route. *ACS Nano* **18**, 16151–16165 (2024).
23. X. Han *et al.*, Plug-and-play assembly of biodegradable ionizable lipids for potent mRNA delivery and gene editing in vivo. bioRxiv [Preprint] (2025), 10.1101/2025.02.25.640222 (Accessed 23 May 2025).
24. X. Han *et al.*, Fast and facile synthesis of amidine-incorporated degradable lipids for versatile mRNA delivery in vivo. *Nat. Chem.* **16**, 1687–1697 (2024).
25. X. Han *et al.*, In situ combinatorial synthesis of degradable branched lipidoids for systemic delivery of mRNA therapeutics and gene editors. *Nat. Commun.* **15**, 1762 (2024).
26. K. Paunovska *et al.*, A direct comparison of in vitro and in vivo nucleic acid delivery mediated by hundreds of nanoparticles reveals a weak correlation. *Nano Lett.* **18**, 2148–2157 (2018).
27. M. M. Billingsley *et al.*, Orthogonal design of experiments for optimization of lipid nanoparticles for mRNA engineering of CAR T cells. *Nano Lett.* **22**, 533–542 (2022).
28. K. L. Swingle *et al.*, Amniotic fluid stabilized lipid nanoparticles for in utero intra-amniotic mRNA delivery. *J. Controlled Release* **341**, 616–633 (2022).
29. K. Chen *et al.*, mRNA vaccines against SARS-CoV-2 variants delivered by lipid nanoparticles based on novel ionizable lipids. *Adv. Funct. Mater.* **32**, 2204692 (2022).
30. C. Hald Albertsen *et al.*, The role of lipid components in lipid nanoparticles for vaccines and gene therapy. *Adv. Drug Deliv. Rev.* **188**, 114416 (2022).
31. K. J. Hassett *et al.*, mRNA vaccine trafficking and resulting protein expression after intramuscular administration. *Mol. Ther. Nucleic Acids* **35**, 102083 (2023).
32. R. de Alwis, S. Chen, E. S. Gan, E. E. Ooi, Impact of immune enhancement on Covid-19 polyclonal hyperimmune globulin therapy and vaccine development. *eBioMedicine* **55**, 102768 (2020).
33. X. Han *et al.*, Adjuvant lipidoid-substituted lipid nanoparticles augment the immunogenicity of SARS-CoV-2 mRNA vaccines. *Nat. Nanotechnol.* **18**, 1105–1114 (2023).
34. S. J. Shepherd *et al.*, Throughput-scalable manufacturing of SARS-CoV-2 mRNA lipid nanoparticle vaccines. *Proc. Natl. Acad. Sci.* **120**, e2303567120 (2023).